GA–A24120

ACCEPTABLE ELM REGIMES FOR BURNING PLASMAS

by

A.W. LEONARD, T.H. OSBORNE, M.E. FENSTERMACHER, R.J. GROEBNER, M. GROTH, C.J. LASNIER, M.A. MAHDAVI, T.W. PETRIE, P.B. SNYDER, J.G. WATKINS, and L. ZENG

SEPTEMBER 2002

DISCLAIMER

GA–A24120

ACCEPTABLE ELM REGIMES FOR BURNING PLASMAS

by

A.W. LEONARD, T.H. OSBORNE, M.E. FENSTERMACHER,*
R.J. GROEBNER, M. GROTH,* C.J. LASNIER,* M.A. MAHDAVI,
T.W. PETRIE, P.B. SNYDER, J.G. WATKINS,† and L. ZENG‡

This is a preprint of a paper to be presented at the 19th IAEA Fusion Energy Conference, October 14–19, 2002, Lyon, France, and to be published in the *Proceedings (CD-Rom).*

*Lawrence Livermore National Laboratory, Livermore, California.
†Sandia National Laboratories, Albuquerque, New Mexico.
‡University of California, Los Angeles, Los Angeles, California.

Work supported by
U.S. Department of Energy under
Contracts DE-AC03-99ER54463, W-7405-ENG-48,
DE-AC04-94AL85000, and Grant DE-FG03-01ER54615

GENERAL ATOMICS PROJECT 30033
SEPTEMBER 2002

Acceptable ELM Regimes for Burning Plasmas

A.W. Leonard,[1] T.H. Osborne,[1] M.E. Fenstermacher,[2] R.J. Groebner,[1] M. Groth,[2]
C.J. Lasnier,[2] M.A. Mahdavi,[1] T.W. Petrie,[1] P.B. Snyder,[1] J.G. Watkins[3] and L. Zeng[4]

[1]General Atomics, P.O. Box 85608, San Diego, California 92186-5608
email: leonard@fusion.gat.com
[2]Lawrence Livermore National Laboratory, P.O. Box 808, Livermore, California 94551
[3]Sandia National Laboratories, P.O. Box 5800, Albuquerque, New Mexico 87185
[4]University of California, Los Angeles, Box 951597, Los Angeles, California 90095-1597

Abstract. The reduction in size of Type I ELMs with increasing density is explored in DIII–D for the purpose of more reliable extrapolation to a burning plasma scale tokamak. The separate convective and conductive transport of energy due to an ELM is determined by Thomson scattering measurements of electron density and temperature in the pedestal. The conductive transport across the separatrix during an ELM is seen to decrease with increasing density, while the convective transport remains nearly constant. The scaling of the conducted ELM energy loss is found consistent with edge MHD stability modeling. Scrape-off-layer (SOL) and divertor diagnostics also show evidence of conductive transport in the SOL at low density with a more convective behavior at high density. Evidence of radial particle transport to the main chamber during an ELM is also presented.

1. Introduction

In a future tokamak burning plasma the ELM energy deposition on the divertor target plates must be maintained below a critical threshold to avoid unacceptable erosion of the target surface [1,2]. The search for a tolerable ELM regime for a burning plasma has taken two approaches. One path seeks to identify ELM free operation that may be accessible to a burning plasma, such as QH–mode observed in DIII–D [3], EDA-mode in Alcator C-mod [4], and the grassy ELM regime of JT-60U [5]. The other option is to determine if the robust Type I ELM regime will in fact produce tolerable ELMs at the pedestal and edge parameters expected in a burning plasma. For ITER, the energy lost from the confined plasma should be no more than 5%–10% of the pedestal energy, given by the pedestal pressure times the plasma volume[2]. Type I ELMing regimes satisfying this constraint have been observed in DIII–D and other devices when operated at high density [6,7]. This paper examines ELM scaling in DIII–D to study the underlying physical mechanisms of ELM energy transport, and in turn how that loss projects to future burning plasmas.

In Section 2 a diagnostic method is described for using Thomson scattering to separately measure energy convected and conducted from the core plasma due to an ELM. In Section 3 ELM conducted and convected energy versus density is presented. A comparison with MHD modeling is made. In Section 4 the scrape-off-layer (SOL) and divertor parallel transport of ELM energy is examined. Section 5 contains a discussion of the results presented.

2. ELM Energy Measurement

The energy lost from the core plasma due to an ELM can be measured on DIII–D by use of the Thomson scattering diagnostic. On DIII–D a fast measurement of the radial profile of T_e and n_e is produced every ~12 ms. The electron density and temperature profiles are ordered and fitted in time with respect to the nearest ELM for steady-state conditions to determine the perturbation to the profiles due to an average ELM. Typical ELM perturbations to the electron temperature and density profiles are shown in Fig. 1(a) and 1(b).

The Δn_e and ΔT_e profiles are integrated over the plasma volume to determine the total ELM energy loss. The ELM energy is split into two channels, a temperature perturbation that represents a conductive process and a density perturbation for convective loss. The convected electron energy is given by integrating $3/2\langle T_e\rangle\Delta n_e$ over the plasma volume. Similarly, the conducted electron energy is given by integrating $3/2\langle n_e\rangle\Delta T_e$. The convected ion energy is assumed to be the same as that of the electrons. This assumption implies Z_{eff} ~1 and $T_i = T_e$.

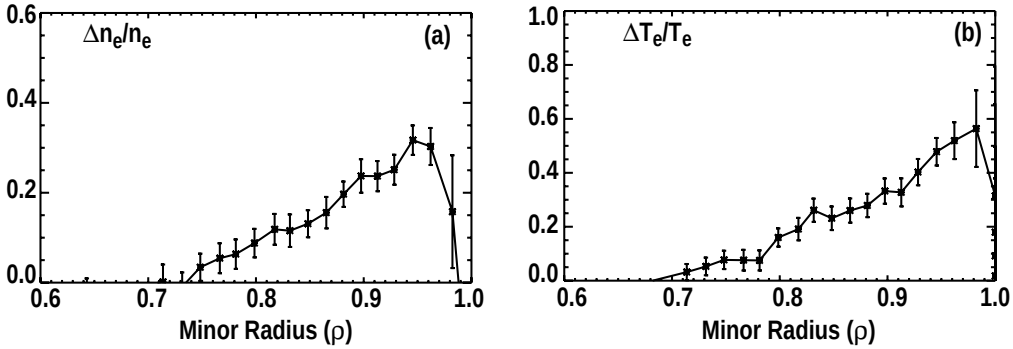

Fig. 1. Thomson scattering measurement of the relative perturbation to the edge (a) n_e and (b) T_e profiles due to an "average" individual ELM. A positive value represents a drop in profile measurement.

For the conducted ion energy, Fast CER measurements with 0.5 ms integration time, show that T_i in the pedestal does drop at an ELM, but only about 1/4 as much as T_e. Therefore we will ignore the conducted ion energy. These approximations can be corrected with future measurements of Z_{eff} and the relation between ΔT_i and ΔT_e. The calculation of ELM energy described above using Thomson scattering produces reasonable agreement with fast equilibrium analysis. Both methods produce scatter in the measurement of ~25%.

3. ELM Energy Lost From Pedestal

The measurement of ELM energy was carried out for four different cases in a lower single-null divertor configuration; (1) q_{95} ~ 3.9 at 1.2 MA and 2.1 T, (2) q_{95} ~ 3.1 at 1.2 MA and 1.5 T, (3) q_{95} ~ 2.5 at 2.0 MA and 2.1 T and (4) q_{95} ~ 4.3 at 1.2 MA and 2.1 T and upper triangularity, δ ~ 0.4 (δ ~ 0 in the other cases). The lower divertor triangularity was δ ~ 0.0 for all cases. The convected and conducted ELM energies are calculated as described above and then normalized by the pedestal energy. The convected, Fig. 2(a), and conducted, Fig. 2(b) energies are then plotted versus the density normalized by the Greenwald density, $n_{GW}(10^{20}m^{-3})= I_p(MA)/[\pi a^2(m)]$. Several important observations can be made in Fig. 2. First, though there is significant scatter in the data there is no obvious trend in the relative convected ELM energy from low density up to $n_{e,ped}/n_{GW}$ ~ 0.65 where the ELMs become smaller. There is also no obvious q_{95} dependence among the different cases. It should also be noted that the higher current and higher triangularity cases have about a factor of 2 higher pressure pedestal, but the ELM energy remains a constant fraction of the pedestal energy.

The conducted ELM energy, however, shows a clear trend with density. The conducted ELM energy is highest at low density and decreases with density to near zero at $n_{e,ped}/n_{GW}$ ~ 0.7. At high density the scatter is due in part to the degradation in pedestal pressure at high

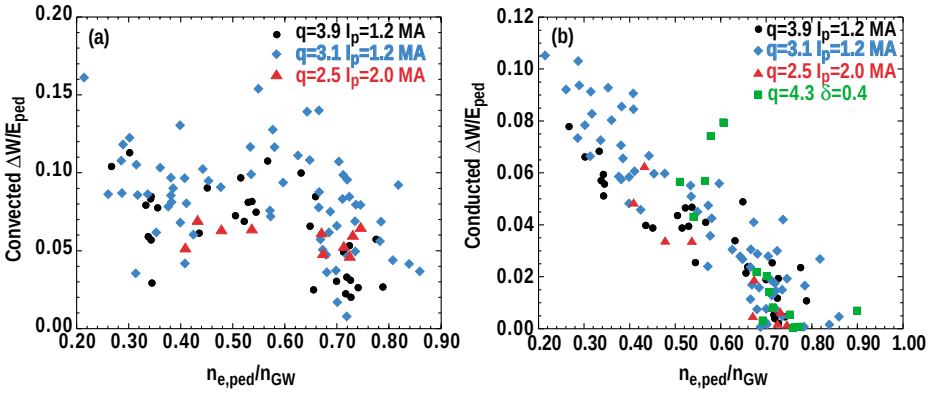

Fig. 2. (a) The normalized convected ELM energy as measured by the Thomson profile versus the pedestal density normalized by the Greenwald density, $n_{e,ped}/n_{GW}$. (b) The normalized conducted ELM energy versus the normalized pedestal density.

density. This results in small ELMs near the measurement sensitivity and a large scatter in the relative ELM size. All four cases follow the same trend within the data scatter. This implies a similar density dependence for the conducted energy regardless of q_{95}, plasma current, triangularity or the pedestal pressure.

The edge stability to peeling-ballooning modes has been examined for several of the discharges of Fig. 2 using the ELITE code [8,9]. It has been suggested that larger ELMs result from longer wavelength modes with an eigenmode structure that extends farther into the main plasma. Modeling was done to determine if edge MHD stability is consistent with decreased ELM size at high density. The ELITE code predicts the growth rate and eigenmode structure of edge peeling-ballooning modes using the measured edge pressure gradients and reconstructed magnetic equilibrium. A collisional bootstrap current model is assumed for the edge current density. The ELITE code predicts similar characteristics for both the low and high current cases with the most unstable mode at n ~40 for low density and increasing to n ~50 at high density. Also the radial width of the eigenmode decreases from ~4% of the minor radius at low density to ~2% at high density. Both of these characteristics, shorter wavelength and narrow instability region, should be consistent with smaller ELMs at higher density through less ergodization of the plasma boundary. The changes to edge stability at high density and collisionality arises first from a reduction in the edge bootstrap current which stabilizes higher order modes. The radial width of the high pressure gradient is also experimentally observed to decrease at high density. This causes the eigenmode structure to narrow and also favors higher-order modes. If the ELM energy is reduced due to a change in the MHD unstable mode then both these factors, pedestal collisionality and pedestal width, are likely involved.

Though the current MHD theoretical analysis may predict an unstable mode and its spatial structure, it does not specify how the mode evolves or transports energy. This theoretical model cannot describe the experimentally observed differences in convected and conducted ELM energies. A model describing the nonlinear evolution of the mode and transport on both the open and closed flux surfaces will be needed to address this topic.

4. SOL and Divertor Response to ELM Flux

Though edge stability is likely necessary for understanding scaling of ELM loss from the core plasma, SOL and divertor transport are important in determining how the lost energy and particles are distributed at the divertor target and plasma facing components (PFCs). Transport in the SOL and divertor could also, in principle, limit ELM energy loss from the core plasma. A simple argument would suggest that parallel transport of ELM energy in the SOL is limited to the ion sound speed [10–12]. Hot electrons transported across the separatrix at the ELM onset should quickly reach the target, within ~10 μs. The loss of electrons quickly builds a sheath potential which limits the loss of ELM thermal energy through parallel electron conduction. The ELM heat flux is then set by the local ion recycling flux at the target. The bulk of the ELM energy would arrive at the target with the ions from the pedestal traveling at the ion sound speed. The spatial profile of the ELM deposition would be set by the ratio of perpendicular to parallel transport.

At low density in DIII–D there is significant evidence that ELM parallel heat flux is not limited by the flow of ions from the pedestal to the divertor. A density scan was carried out on DIII–D in a lower single-null configuration that optimized the views of a number of fast diagnostics. The behavior of several of these parameters at low density are shown in Fig. 3. For the low density discharge the pedestal parameters are $T_{e,ped}$ ~750 eV and $n_{e,ped}$ ~5×10^{19} m^{-3} representing an ion sound speed time from the outer midplane to the outer and inner targets of ~50 μs and ~120 μs respectively. The first indication of rapid parallel transport of electron energy is the fast drop in SXR emission from the pedestal. The SXR signal indicates the drop in pedestal T_e, as seen previously in Fig. 1, occurs in ≤ 100 μs, the time resolution of the SXR diagnostic.

Other diagnostics shown in Fig. 3 indicate the ELM power pulse is arriving simultaneously to both divertors. The inboard and outboard divertor D_α signals rise together as does the ion saturation current at the divertor target. The resulting target heat flux as measured by IR emission is also simultaneous and of similar magnitude in both the inboard and outboard divertors. However, the time resolution of these diagnostics ≤ 100 μs and time difference between the divertors due to ion sound speed flow would be barely observable.

An indication of how significant electron energy conduction might occur before the pedestal ions reach the target is shown by the temporal evolution of the outboard density in the last trace of Fig. 3. The CO_2 interferometer measures the line integral of density on a vertical path through the main plasma and outboard divertor. The density along this path averaged over a number of ELMs rises from a value of $1.4\times10^{19}m^{-2}$ before the ELM to a peak value of $\geq 1.8\times10^{19}m^{-2}$ in < 100 μs during an ELM. The rise in divertor density at an ELM is estimated at $\geq 2\times10^{20}m^{-3}$ given a path length of 18 cm through the divertor and the assumption that the density does not rise in the main plasma during an ELM. Before an ELM the divertor density is ~ $4\times10^{19}m^{-3}$ as measured by Thomson scattering. The rise in divertor density is much greater than either the pedestal density or the pre-ELM divertor density indicating local generation of plasma at the target. One possible source of particle generation is each local ion falling through a much larger sheath could dislodge several neutrals from the target allowing for a rapid buildup of density and particle flux. The increased particle flux at the target would then allow a greater level of electron heat conduction before the arrival of ion flux from the pedestal.

At high density a slower evolution of the SOL and divertor response to an ELM is observed in Fig. 4. The pedestal parameters in this case are $T_{e,ped}$ is ~300 eV and $n_{e,ped}$ ~$1\times10^{20}m^{-3}$. At high density the divertor Dα and ion saturation current exhibit a slower rise and longer duration peak than at low density. The duration of the inboard heat flux is also longer, but with a much smaller outboard heat flux. A larger inboard than outboard ELM heat flux has also been reported earlier [1] though it is still not understood. Finally the outboard divertor density behavior is opposite to the low density case and decreases at an ELM. Before the ELM the outboard divertor is in a cold dense state, $T_e \leq 5$ eV and $n_e \approx 4\times10^{20}$ m^{-3}. The ELM heat pulse heats the cold dense plasma and electron pressure balance likely pushes some of the high density plasma back up the SOL at the ion sound speed.

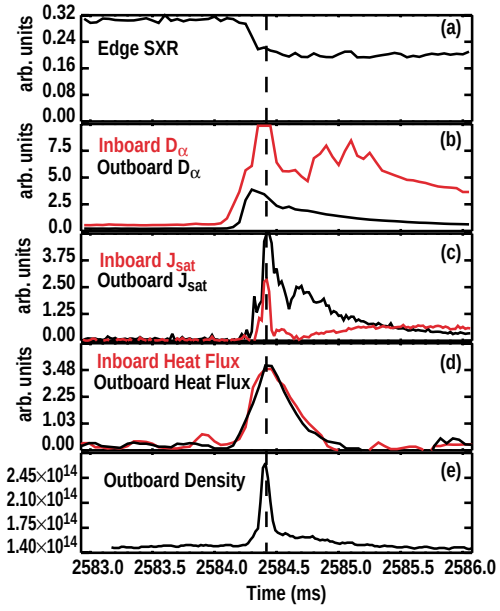

Fig. 3. Fast timescale response of divertor diagnostics at low density. Shown are (a) the pedestal SXR signal, (b) inner and outer divertor D_α, (c) inner and outer divertor particle flux from Langmuir probes, (d) inner and outer divertor heat flux and (e) divertor density measured by a CO_2 interferometer.

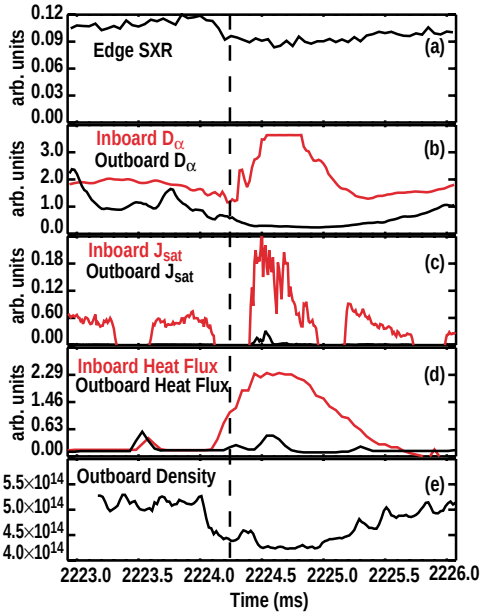

Fig. 4. Divertor diagnostics response to an ELM at high density. Diagnostics shown are the same as in Fig. 3.

There is also evidence of significant radial transport in the SOL during an ELM. At low density a rapid rise in the midplane SOL is observed with Thomson scattering and microwave profile reflectometry. These diagnostics indicate a rise in density of $\geq 1\times10^{19}$ m^{-3} out to > 4 cm outside the separatrix at the midplane within 500 μs of the ELM instability. The decay time of the SOL density after an ELM is 1–2 ms. The integral of the rise in density around the plasma periphery is roughly equal to the density loss of the pedestal at each ELM. These SOL observations indicate ions from the pedestal undergo rapid radial transport during an ELM with a large flux out to the main chamber wall. However, the width of the divertor heat flux due to an ELM is measured to be 1–2 times the steady state heat flux width. The observation of narrow heat flux on the divertor target simultaneous with significant main chamber flux is also suggestive of electron conduction as the channel for ELM divertor heat flux.

5. Summary

At high density in DIII–D ELMs become more benign. Not only is the energy loss smaller at high density, but the deposition time for the ELM energy on the divertor target is also longer. The small ELMs at high density in DIII–D are within a tolerable range when scaled to ITER. It is important to understand the processes that lead to these small ELMs in order to adequately predict operation in a future burning tokamak. MHD analysis of these discharges suggest that smaller ELMs at high density result both from a loss of edge bootstrap current at higher collisionality, and a narrower pedestal. A burning plasma will have a low collisionality pedestal which would suggest large ELMs. However, the scaling of the pedestal width to a burning tokamak is still uncertain and could significantly affect ELM size. Finally, though the linear stability of ELM modes has been correlated with ELM size, this MHD model cannot follow the nonlinear evolution of the mode, nor describe the resulting transport. Further refinement of the MHD model is needed to improve the understanding and reliability of scaling these results.

The SOL and divertor measurements also indicate that the reduction in lost electron temperature from the pedestal at high density is likely due to a reduction in the ELM instability and not a limitation of SOL parallel transport. At high density the ELM heat flux deposition time becomes longer, consistent with convective transport from the pedestal across the separatrix and ion sound speed flow in the SOL to the divertor. This should lead to longer deposition times in a burning plasma with a longer path length from the midplane to the divertor. One final concern is the main chamber fluxes due to an ELM. Because of the long equilibration times any ion lost from the pedestal will likely carry much of its energy to the wall or target. If a fraction of the ion flux is spread evenly about the main chamber this could be beneficial. However, if the flux is localized to a small area, damage to plasma facing components is possible.

Acknowledgment

Work supported by U.S. Department of Energy under Contracts DE-AC03-99ER54463, W-7405-ENG-48, DE-AC04-94AL85000, and Grant DE-FG03-01ER54615.

References

[1] A.W. Leonard, A. Herrmann, K. Itami, *et al*., J. Nucl. Mater. **266-269** (1999) 109.
[2] G. Federici, et al., accepted for publication in J. Nucl. Mater.
[3] K.H. Burrell, M.E. Austin, D.P. Brennan, , *et al*., Plasma Phys. and Cont. Fusion **44** (2002) A253.
[4] M. Greenwald, *et al*., Plasma Phys. and Cont. Fusion **42** (2000) A263.
[5] Y. Kamada, *et al*., Plasma Phys. and Cont. Fusion **42** (2000) A247.
[6] A.W. Leonard, R.J. Groebner, M.A. Mahdavi, *et al*., Plasma Phys. and Cont. Fusion **44** (2002) 945.
[7] J. Stober, M. Maraschek, G. D. Conway, *et al*., Nucl Fusion **41** (2001) 1123.
[8] J.W. Conner, *et al*., Phys. Plasmas **5** (1998) 2687.
[9] P.B. Snyder, H.R. Wilson, J.R. Ferron, *et al*., Phys. Plas. **9** 2037 (2002).
[10] A. Loarte, accepted for publication in J. Nucl. Mater.
[11] A. Herrmann, accepted for publication in J. Nucl. Mater.
[12] A. Bergmann, accepted for publication in Nucl. Fusion.